



BIO-NANOCOMPOSITE FILMS BASED ON CELLULOSE NANOCRYSTALS FILLED POLYVINYL ALCOHOL/ALGINATE POLYMER BLEND

¹Houssine Khalili, ¹Mohamed Hamid Salim, ¹Sif-eddine Jabor Tlemceni, ¹Rachid Makhlouf, ¹Fatima-Zahra Semlali Aouragh Hassani, ¹Houssine Ablouh, Zineb Kassab, ¹Mounir El Achaby*

¹Materials Science, Energy and Nanoengineering Department (MSN), Mohammed VI Polytechnic University (UM6P), Lot 660 – Hay Moulay Rachid, 43150, Ben Guerir, Morocco.

*Corresponding author

Email: mounir.elachaby@um6p.ma

Abstract. *In this work, the Juncus plant was used as an abundant and sustainable raw material for the production of cellulose nanocrystals (CNC). Herein, cellulose nanocrystals were prepared via sulfuric acid hydrolysis exhibiting a needle-like shape morphology, with an average diameter of 6.8 ± 1.8 nm and length of 457 ± 76 nm, arising to an aspect ratio of 59. Moreover, X-ray diffraction and TGA show that the CNCs exhibit high crystallinity and good thermal property respectively compared to other sources. Further investigation was conducted by preparing novel bio-nanocomposites through the incorporation of CNCs into the polyvinyl alcohol-alginate (PVA-ALG) blend matrix. Thus, giving enhanced properties compared to the pure matrix, particularly the mechanical properties due to the good interfacial adhesion, confirmed by FTIR analysis, while maintaining good transparency at low CNCs concentration, which is required for packaging application.*

Keywords: *Juncus plant; cellulose nanocrystals; PVA-ALG blend; bionanocomposites film.*

1. Introduction

In recent years, an increasing interest in biodegradable or sustainable polymers and environmentally friendly materials as a whole has been generated by current concerns about environmental pollution and the decreasing availability of petroleum [1,2]. Consequently, biopolymers have caught the interest of academics due to their potential applications in a variety of industries, including food packaging, pharmaceuticals, the automobile industry, and cosmetics [3–5]. The mechanical, optical, processing, and thermal qualities of biopolymers need to be improved in order for them to compete with petroleum derivatives, despite the fact that they have shown some promise [2]. The most common methods for the reinforcement of the biopolymer are solution blending and nanofiller reinforcement [6–8].

The blending of the polymer by combining two or more natural biopolymers (alginate [9,10], chitosan [11], starch [3,7], gelatin [12], etc.) and synthetic polymers (polyvinyl alcohol [13], poly(ethylene oxide) [14], polylactic acid [15], etc.) results in the creation of new composite materials

with improved or unique qualities that are used in various fields. Polyvinyl alcohol (PVA) is a basic linear hydrophilic synthetic polymer containing hydroxyl pendant groups and is commercially manufactured from polyvinyl acetate [11]. PVA is used in a wide range of industrial and packaging applications because of its film-forming properties, optical transparency, biodegradability, high crystallinity, and mechanical properties [1,16]. In general, PVA is one of the widely available synthetic polymers and has a relatively low manufacturing cost and environmental impact [17].

Brown seaweed is a source of alginate (ALG), a naturally occurring and biodegradable polymer that is negatively charged [6,18]. Researchers have given particular interest to ALG due to its extraordinary biocompatibility, low toxicity, and film-forming ability at room temperature [19,20]. In comparison to PVA, ALG has significant drawbacks, including a high hydrophilic nature, poor heat stability, and poor mechanical qualities, all of which severely limit its applicability [21,22]. Therefore, an appropriate solution, such as PVA-ALG solution blending, is required to improve desired properties along with biocompatibility. Eghbalifam et al. reported that the addition of ALG led to a remarkable increase in rigidity of PVA-ALG blend composite with a tensile modulus of 710 MPa and tensile strength of 45 MPa [23]. Another study showed that by adding more ALG to the PVA-ALG blend, it was possible to produce improved thermal stability and a better beginning temperature of deterioration over 350°C [10]. Similarly, Jiang et al. prepared PVA-ALG blend composite with elongation at break of 400%, a tensile strength of 1.32 MPa, and conductivity of 3.62 S/m [21].

Another important technique for improving the desired properties of polymeric materials is nanofiller technology, which is a promising way to enhance polymers and blend polymers materials' mechanical, thermal, and barrier properties [4,5]. Nanotechnology involves filling in a polymer matrix with inorganic or organic nanoparticles such as nanocellulose [24,25], nanoclays [17], and nanometals [23], to overcome their disadvantages. Cellulose nanocrystals (CNCs) are among the best nanofiller agents due to their outstanding properties and compatibility with biopolymers [26,27]. CNCs are extracted from abundant natural resources and have large surfaces with excellent structural, mechanical, thermal, and optical properties, which are the parameters needed for various applications, including packaging [28,29]. Nanocomposite films based on PVA containing 8 wt.% CNC demonstrated an increase of 107% and 78% for tensile modulus and tensile strength, respectively compared to neat PVA [30]. Popescu et al. reported that at low CNC content in the PVA matrix, the crystallinity degree decreased to 29.9% [31]. In comparison, the degree of crystallinity increased to 80.6 % at higher CNC content compared to PVA (35.4%) [31]. Similar to this, when 8 wt.% of CNCs were added to the ALG matrix, the modulus, strength, and toughness increased from 1310 to 2846 MPa (117%), from 50 to 97 MPa (94%), and from 5.3 to

8.3 MJ/m³ (56%), respectively [18]. Another study of ALG-CNC bio-nanocomposite films revealed that the inclusion of CNCs did not significantly alter the thermal degradation because of the CNCs' fine dispersion and the subsequent development of a complex network due to strong interactions between the CNCs' surface functionality and the macromolecular chains of ALG [19].

In the present study, a blend of two biodegradable polymers (polyvinyl alcohol and alginate) was tested to prepare composite films reinforced by CNCs. To the best of our knowledge, CNCs were used for the first time, as reinforcing fillers in PVA-ALG based blend films. Hence, this study also aimed to explore the use of the *Juncus* plant as a source of raw material for CNC production using sulfuric acid hydrolysis. PVA-ALG-CNC nanocomposite films were produced from mixtures of PVA-ALG blend and CNC suspensions using the solution casting method. The main objective was to examine the CNC nanofiller effect on the morphological, structural, optical, thermal, and mechanical properties of the PVA-ALG matrix in determining the potential use of PVA-ALG-CNC films as green packaging material.

2. Methods

2.1. Materials

Raw *Juncus* plant was obtained from the region of Settat, Morocco. The as-received raw *Juncus* plant with a length of approximately 1200 mm was cut into small fibers of 2-4 cm in length; then, they were ground using a home coffee mill. Polyvinyl alcohol (PVA) (Mw 130000, 99+% hydrolyzed), Alginate (ALG) (Alginic acid sodium salt from brown algae with medium viscosity, CAS 9005-38-3), and all other chemicals were purchased from Sigma-Aldrich and used as received.

2.2. Cellulose nanocrystals extraction

In order to extract cellulose nanocrystals (CNCs), cellulose microfibrils were first obtained from ground raw *Juncus* plant using three well-known steps: hydrothermal, alkali and bleaching treatment. CNCs were extracted from the obtained cellulose microfibrils using sulfuric acid hydrolysis treatment. The hydrolysis process was conducted under magnetic agitation with a solution of sulfuric acid (64 wt.% concentration) at a constant temperature of 50 °C for a duration of 30 min. The obtained CNC were used as a nano-filler for PVA-ALG based composite films.

2.3. Nanocomposites films preparation

In this study, PVA-ALG blend films reinforced with different concentrations of CNC (2.5, 5, and 10 wt.%) and without CNC were prepared by solvent casting method. Initially, PVA powder was dissolved in distilled water at 90°C for 2 hours under mechanical stirring, left to cool, and

then ALG powder was added into the solution (at the weight ratio of PVA:ALG = 4:1) and mixed for 2 hours at room temperature. Simultaneously, suspensions of CNC were measured and sonicated for 15 min to disperse any agglomerates formed. The CNC suspensions were then poured into the blend of PVA-ALG and mixed under mechanical stirring at room temperature for 5 mins. Finally, the obtained solutions were cast into a petri dish and left to evaporate at room temperature. The dried films were removed from the Petri dish and used for further analysis. For comparison purposes, pure PVA, and PVA-ALG blend films were also prepared using the same method without the addition of CNC. The PVA-ALG nanocomposite films were coded as PVA-ALG-2.5CNC, PVA-ALG-5CNC, and PVA-ALG-10CNC. The number in each code name indicates the CNC weight fraction in each formulation of the nanocomposite film. The film thickness was determined by using the hanatekvariable force precision thickness gauge (FT3-V), at ten random locations of the tested film samples. The thickness was measured to be 0.065, 0.066, 0.067, 0.068 and 0.069 mm for neat PVA, PVA-ALG, PVA-ALG-2.5CNC, PVA-ALG-5CNC, and PVA-ALG-10CNC, respectively. It was noticed that when CNC concentration increased, the thickness of the films slightly increased due to the increasing solid content. This result is in line with other studies that showed the thickness of CNCs-based nanocomposite films increased as CNCs concentration increased [25,28]. It is worth noting that the thickness of the films was controlled by pouring a constant volume (100 mL) of the blend solution into the dish.

2.4. Characterization techniques

In order to get information regarding the dimensions and shape of CNC, Atomic force microscopy (AFM) was used for this purpose. For that, CNC suspension of 0.01 wt% was homogenized by using an ultrasonication device for 15 min and then deposited on a mica sheet. Veeco Software data analyzer was used to determine CNC dimensions. To study the chemical structure, Fourier-transform infrared (FTIR) spectrum was recorded using Perkin-Elmer spectrum 2000) with an ATR accessory, the studied samples were analyzed in a range of wavelength (4000-600) cm^{-1} . In order to confirm the crystalline structure and to determine the crystallinity index of the samples, X-ray diffraction (XRD) analysis was performed. X-ray diffractometer (D2 phaser diffractometer) was employed using a source of CuK at $\lambda = 1.54056 \text{ \AA}$ (40 kV, 40 Ma), working between $2\theta = 5-50^\circ$ with a scanning rate of $2^\circ/\text{min}$. The crystallinity index (*CrI*) was determined using the Segal equation [28,32,33]. The crystallinity index was measured following the Segal equation:

$$CrI = \frac{I_{200} - I_{amorph}}{I_{200}} \times 100,$$

I_{200} represent the intensity of the diffraction plane (200). At $2\theta = 22^\circ$ correspond to the crystalline region, where I_{amorph} the intensity of the amorphous region at $2\theta = 18^\circ$. The thermal

stability was studied by thermogravimetric analysis (TGA, Discovery TGA from TA instruments); samples were heated from room temperature to 700 °C under a nitrogen atmosphere with a heating rate of 10 °C/min. The optical transparency of the bio-nanocomposite films was measured by PerkinElmer Lambda 1000 spectrophotometer. The films were placed in the chamber test with the air as a reference, and the wavelength ranging from 200 to 800 nm.

The mechanical properties of the films (50 x 10 mm) were determined in the tensile mode (3 batches) with an initial grip separation of 30 mm and a stretching rate of 5 mm/min using the Universal Testing Machine Texture Analyzer (TA. XT plus). The tensile strength (MPa) was determined using the maximum amount of tensile stress divided by the initial cross-sectional area of the film sample.

3. Results and discussion

3.1. Cellulose nanocrystals production

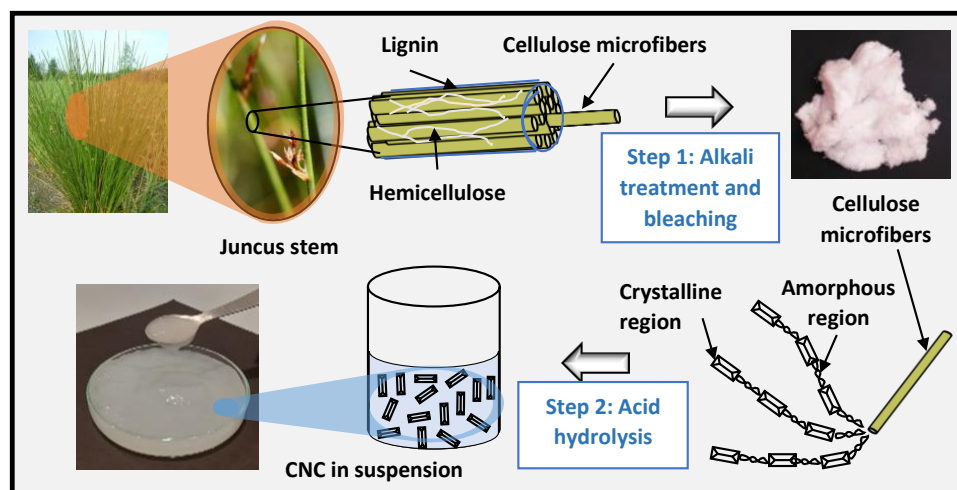


Figure 1. Overall steps and digital images of CNC production

The complete production method of CNC from raw *Juncus* plant is briefly elaborated in the schematic presentation Fig. 1. In the first step through the chemical process i.e. alkali and bleaching processes Fig. 1, raw *Juncus* plant fibers were transformed into cellulose microfibrils. The alkali treatment serves to eliminate non-cellulosic compounds (lignin and hemicellulose) that have sandwiched the cellulose microfibrils [34,35], as shown in Fig. 1. Whereas the bleaching procedure helps to eliminate residual lignin as well as other impurities that remained after alkaline treatment [35]. Eventually, in the second step Fig. 1, the bleached cellulose microfibrils were hydrolyzed with sulfuric acid in such a way that this process allowed amorphous regions to be removed from the cellulose microfibrils and obtain the crystalline regions as proved by the XRD results. Finally, an aqueous stabilized CNC suspension was obtained, as shown in the digital photo

Fig. 1 in which a whitish/transparent gel is observed. It was noted that the obtained CNC stabilizes very well in water after ultrasonication, which is an essential property in the development of nanocomposite films [25,27]. The obtained gel was thereafter dried via lyophilization for morphological, structural, and thermal analysis.

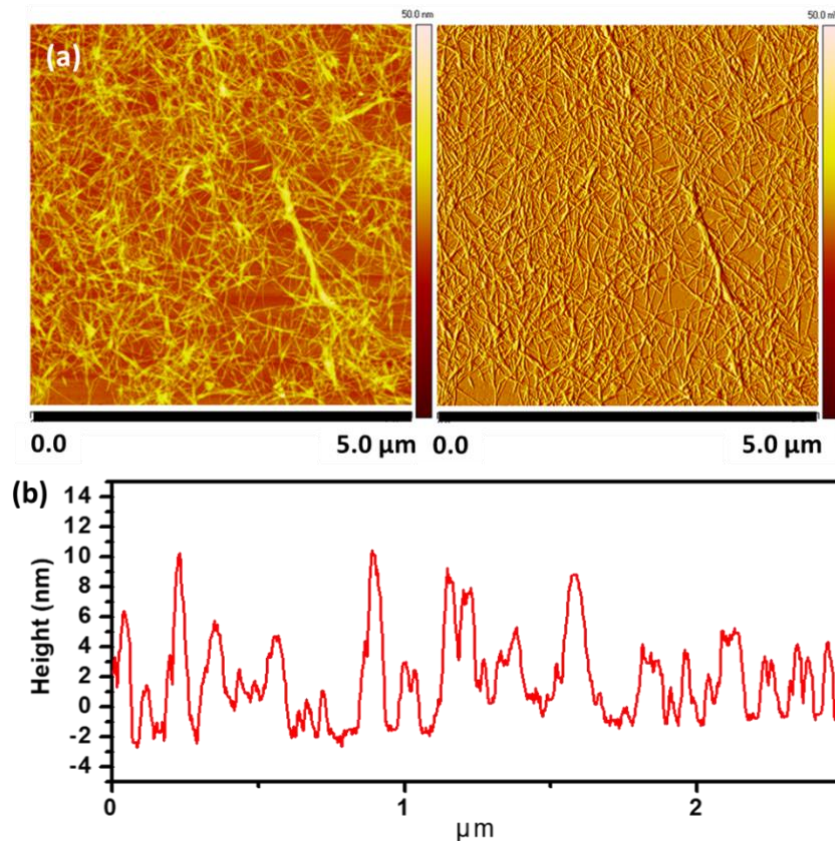


Figure 2. (a) AFM images, and (b) representative height profiles of the as-extracted CNC

3.1.1. Morphological analysis

The AFM analysis was used to confirm the isolation of individual nanocellulose and determine its morphology and measurements of the CNC. Fig. 2 AFM images of CNCs and its height profile, respectively. The AFM images show that as-obtained CNCs by sulfuric acid hydrolysis have a needle-like shape morphology, with an average diameter of 6.8 ± 1.8 nm and length of 457 ± 76 nm, resulting in an aspect ratio of 67. Table 1. provides a comparison of the obtained CNCs measurements with other CNC taken from other sources using the same extraction conditions. Generally, the morphology of CNC strongly depends on the raw bio-materials origin and conditions of extraction [36–38]. For instance, the decrease in CNC diameter and length could be due to the high acidity of used sulfuric acid [24,39]. In this case, the high aspect ratio achieved for our CNCs could be advantageous for better interaction between the nanofiller and polymer matrix.

Table 1. Comparison table of the yield and properties of cellulose nanocrystals derived from various sources

Type	Source	(D) nm	(L) nm	Aspec t ratio	Yield (%)	Cr%	T _{onst} (°C)	T _{max} (°C)	Ref
Conventional sources	Hard wood	14.9	171	11.5	20	61.5	-	185	[40]
	Soft wood	16.9	179	10.6	20.5	64.9	-	192	[40]
	Cotton	25	450	18	77	91		280	[41]
Annual plants	Juncus	7.3	431	59	-	81.3	221	332	This work
	Hemp	21	200	-	19	83	309	354	[42]
	Alfa fibers	5	329	65	-	90	217	340	[18]
	Flax	50.3	305	6.06	-	-	330	363	[43]
	rice straw	15	172	11.46	-	78	185	304	[8]
	Penisetum sinense	20	200	-	-	77	236	332	[44]
Agricultural residue	Tomato	7.4	367	49	-	89	219	329	[45]
	Corncoobs	4.9	287	63.0	57	79.8	200	300	[30]
	Ushar seed fiber	14	140	10	36	70.0	240	350	[46]
	Pineapple crown	39	245	6.3	-	73	124	348	[32]
Industrial residue	Potato peel waste	10	183	18	41	85	-	-	[35]
	Apple pomace	7.9	28	-	28	78	150	300	[47]
	Sugarcane bagasse	5	275	56	-	78	153	230	[13]
	mango seed	4.59	123.4	34.1	22.8	90.6	248	271	[28]
Marine biomass	Brown Sargassum	8.81	43.72	5.05	25.8	83	260	380	[6]
	Algae waste	9	315	35	-	81	201	331	[40]
	Green Sea lettuce	17.3	53.18	3.16	20.3	66.9	300	400	[5]

3.1.2. Structural analysis

CNC's structural analysis is the determinant factor for its thermal and mechanical properties [33,35,42,48]. The CNC's functional surface groups were revealed using FTIR spectroscopy and the CNC's crystalline structure using the XRD technique, as shown in Fig. 3. In the FTIR spectra (Fig. 3a), the band at 3321 cm⁻¹ was attributed to the strong inter- and intra-molecular *H*-bonding. The bands at 2894 cm⁻¹, 1368 cm⁻¹ and 892 cm⁻¹ was attributed to CH stretching vibration in

cellulose, respectively [11,24,25]. Besides, the band at 1310 cm^{-1} and 1435 cm^{-1} were attributed to the CH_2 symmetric bending groups and it is regarded as a crystallinity band in any cellulosic material [13]. The appearance of a band at 1638 cm^{-1} is due to the deformation vibration of OH groups [31]. In addition, the bands observed in the spectra at 1160 cm^{-1} , 1084 cm^{-1} , and 1020 cm^{-1} are associated with C–O–C stretching vibration, C–O pyranose ring skeletal vibration, and C–O cellulose molecule stretching bonds [27]. Most notably, the addition of sulfate groups on the CNC surface in the course of the hydrolysis process was confirmed by a band at 1204 cm^{-1} [31,49].

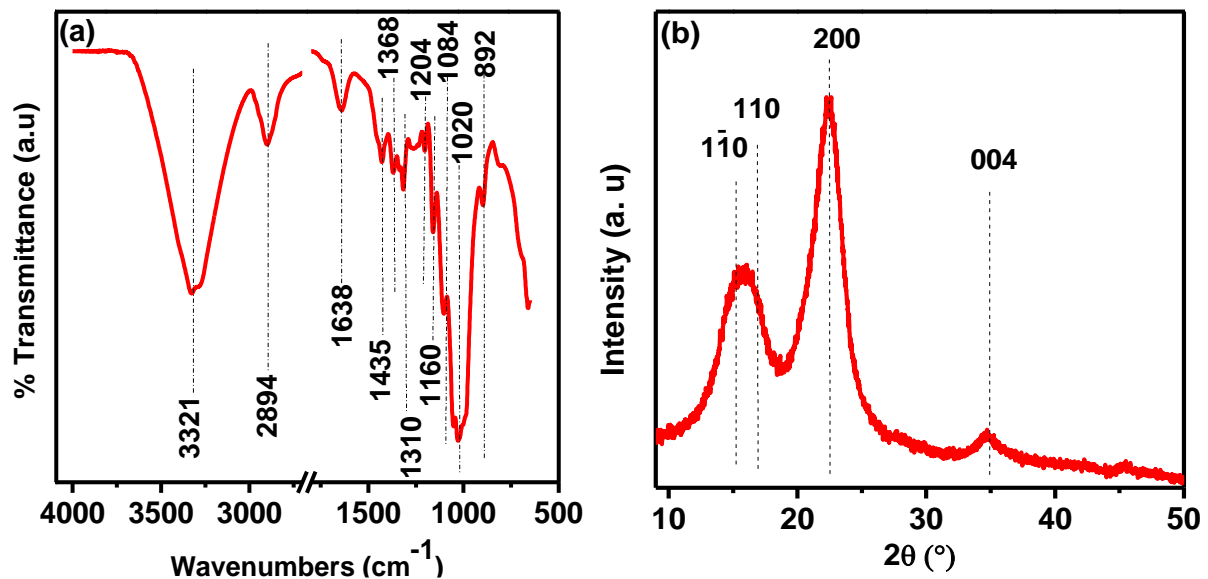


Figure 3. (a) FTIR and (b) XRD of CNC

The XRD pattern of the CNC sample is presented in Fig. 3b, and the calculated crystallinity index (*CrI*) is given in Table 1. The characteristics peaks of cellulose structure I were situated at the 2θ position; 15.21° , 16.87° , 22.46° , and 34.89° corresponding respectively to the cellulose I crystallographic planes ($1\bar{1}0$), (110), (200), and (004). The *CrI* of the CNC sample from the XRD data was determined to be 81.3%. By using the acid hydrolysis extraction method, different CNCs' *CrI* value was reported in the literature as presented in Table 1. The moderately high *CrI* value of CNC from *Juncus* is due to the chemical breakdown of the amorphous part of cellulose microfibrils by the hydrolysis treatment. Interestingly, the high crystallinity of the obtained CNC is an important factor needed to use it as nanofillers for the production of nanocomposites.

3.1.2. Thermal analysis

The TGA/DTG analysis was used to evaluate the thermal stability of the CNC and the results obtained are shown in Fig. 4. The CNC sample was observed to be undergoing a two-step degradation phase. The first degradation phase represents a 5% of loss in mass at nearly 100°C ; this is due to the evaporation of physical moisture at the surface [29,50]. In the second phase, an

important weight decrease is observed in the range of 200–530 °C due to cellulose degradation processes [34,51]. Herein, the thermal stability (T_{onset}) and maximum degradation temperature (T_{max}) were found to be 157 °C and 332 °C, respectively. Nonetheless, the thermal decomposition of the CNC sample resulted in char residue (34%) at 600 °C that could be attributable to intrinsically flame-resistant sulfated cellulose regions [32,33].

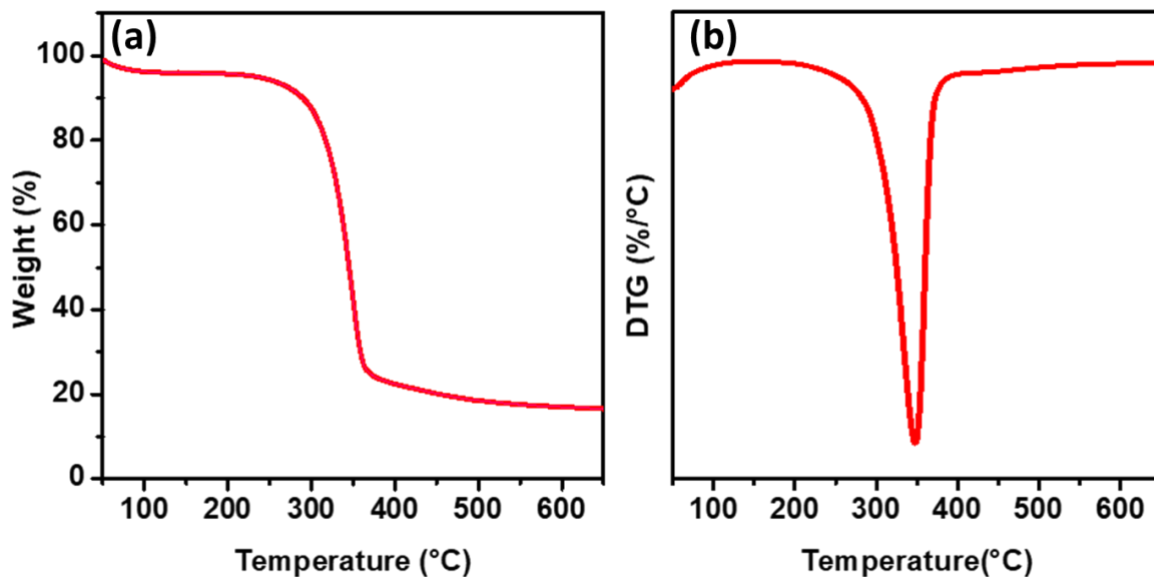


Figure 4. (a) TGA, and (b) DTG curves of CNC

3.2. Bio-Nanocomposites films characterization

3.2.1. Processing of Bio-Nanocomposites and Interfacial Interactions

The interfacial interaction in the polymer blend and their nanocomposites is shown in Fig. 5. Indeed, the availability of the hydroxyl groups in the polymer's surface, leads to the creation of strong hydrogen bonds forming a compatible blend network. Moreover, the addition of CNCs negatively charged surface with sulfate group added more hydrogen bonding to the mixture. Thus, forming a strongly interconnected network.

The FTIR spectra of neat PVA, PVA-ALG, and its nanocomposite films at different CNC weight fractions of 2.5, 5 et 10% were reported in Fig 7. Neat PVA has characteristic peaks at 3337 cm^{-1} , 2941 cm^{-1} , 1709 cm^{-1} , 1092 cm^{-1} , and 850 cm^{-1} which represent the bending vibration of hydroxyl groups, CH_2 , C=O bending vibration, C-O group, and C-C group stretching vibration respectively [22,52]. All the films exhibit approximately the same peaks, with a slit shift in the range of 3600-3000 cm^{-1} indicating the presence of a hydrogen bond among the OH group of PVA and ALG [2,5,20]. In addition, some peak characteristics at 624 cm^{-1} and 1420 cm^{-1} correspond to the stretching vibrations of asymmetric and symmetric COO^- respectively [10]. PVA-ALG-CNC films exhibited also the same bands as the PVA-ALG blend with a small difference, regarding the

addition of CNC into the PVA-ALG matrix that is shown in the shifting of the hydroxyl bands between ($3500\text{-}3000\text{ cm}^{-1}$), in addition to the appearance of the band at 1638 cm^{-1} that is due to the deformation vibration of OH groups and all bands of CNC which is confirmed with FTIR spectra of CNC in the above result. This confirms the compatibility and the interaction between all groups located in PVA, ALG, and CNC which result in the formation of hydrogen bonds between OH and the carboxyl group which is represented in Fig.6. Similar results are observed in several works [11,28,36].

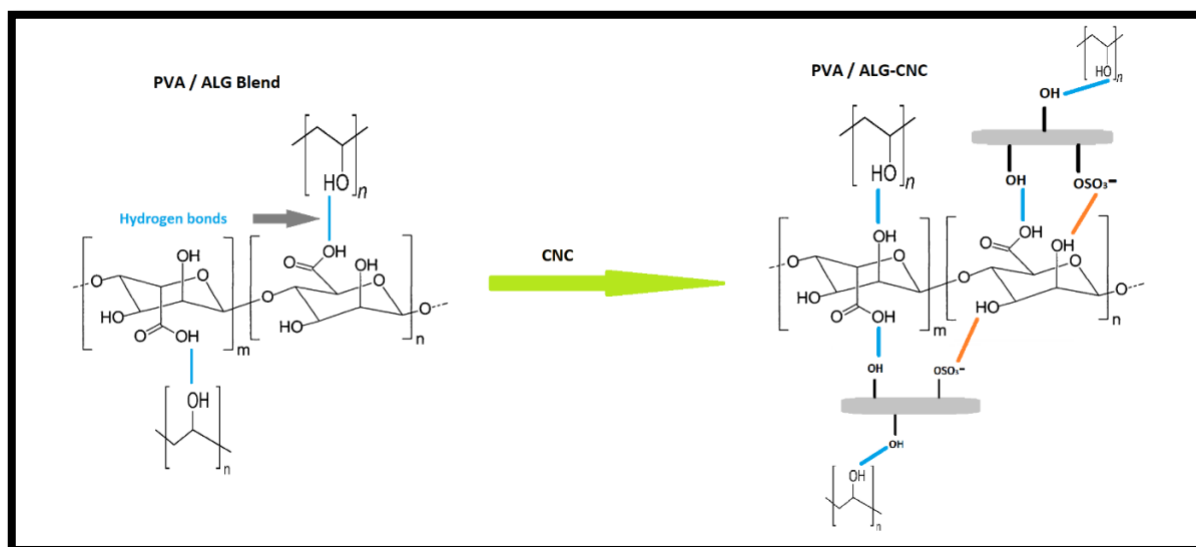


Figure 5. Interaction bonds between PVA, ALG, and CNC

3.2.2. Structural Properties of Bio-Nanocomposite Films

3.2.3. Morphological Properties of Bio-Nanocomposite Films

The surface of the films was investigated using SEM as displayed in Fig. 7. The surfaces of the neat PVA and PVA-ALG films were observed to have a smooth surface Fig. 7a-b. This morphological characteristic suggests that PVA-ALG has high processability and film-forming properties during solvent casting. After the CNC was added as a filler, it was observed that the CNC was evenly distributed throughout the PVA-ALG-2.5CNC and PVA-ALG-5CNC films (Fig. 7c-d). This showed that CNC and the PVA/ALG blend interlinked well together to create homogenous nanocomposite films, which may enhance the characteristics of a bio-nanocomposite film. However, a high CNC concentration (10 wt.%) resulted in the formation of a rough surface, as seen in Fig. 7e. The few agglomerations that appeared within the morphology for the PVA-ALG-10CNC nanocomposite implied that the content of 10 wt.% CNC might influence the structure of the nanocomposite films [3,53].

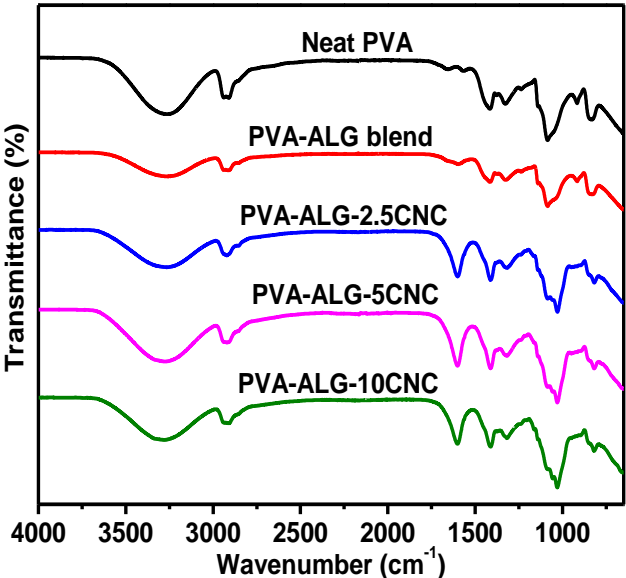


Figure 6. FTIR spectra of neat PVA, PVA-ALG, and its nanocomposite films at different CNC weight fractions 2.5, 5, and 10 wt.%

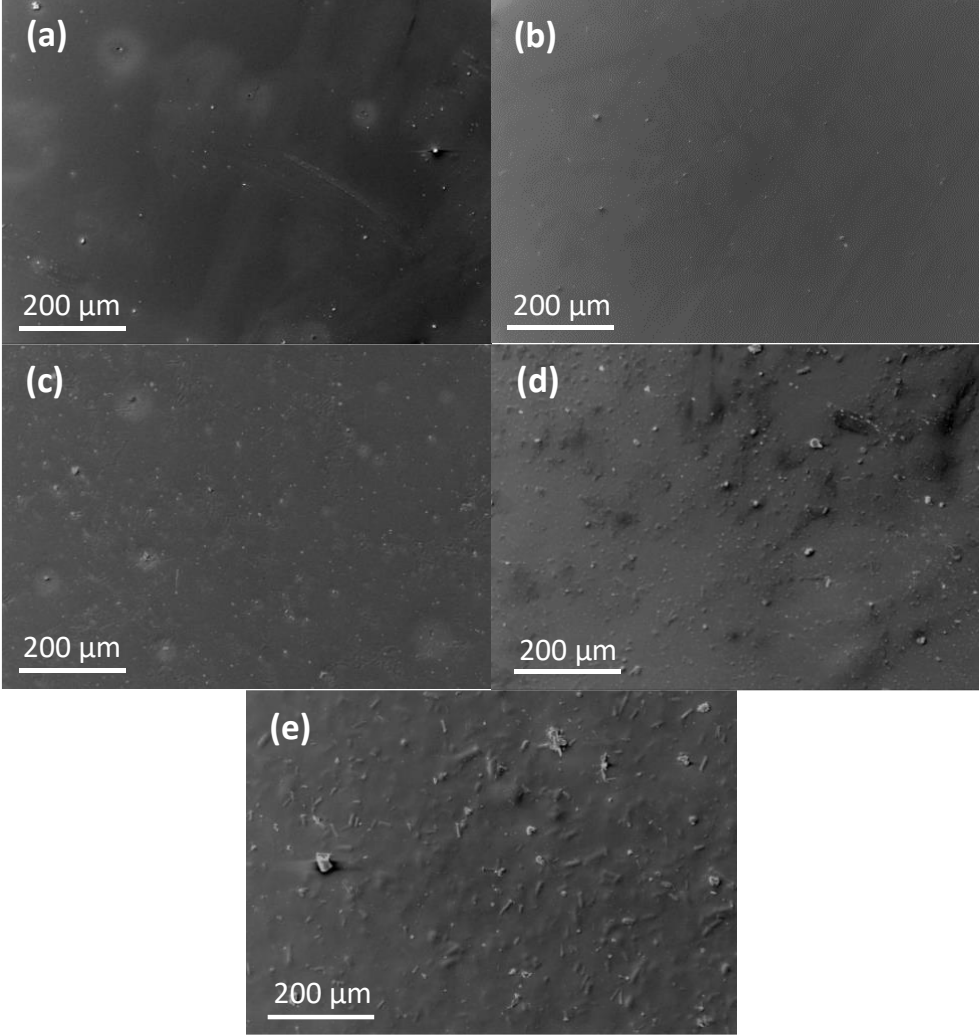


Figure 7. SEM of (a) neat PVA, (b) PVA-ALG blend, (c) PVA-ALG-2.5CNC, (d) PVA-ALG-5CNC, and (e) PVA-ALG-10CNC

3.2.4. Optical Transparency of Bio-Nanocomposite Film

UV-vis spectroscopy was used to measure the optical transparency of nanocomposite films of PVA-ALG matrix filled with different concentrations of CNC and to evaluate the dispersion of CNC within it [54,55]. Transparency is an interesting factor to assess the quality of films for different applications, especially in food packaging [19,29]. The UV-vis transmittance spectra of neat PVA, PVA-ALG, PVA-ALG-2.5CNC, PVA-ALG-5CNC, and PVA-ALG-10CNC are shown in Fig. 8. The Neat PVA is a high transparent biopolymer with a transmittance of 91%, the same value was obtained by other researchers [11,51]. The PVA-ALG based films showed an 84% transmittance, indicating that the addition of ALG had no adverse effects on the PVA films that would have prevented the transparency of the blend films. The transparency of the PVA-ALG film was slightly affected by the addition of 2.5 and 5 wt. % of CNC. This result demonstrates that CNC and PVA-ALG possess great compatibility. This compatibility helps to prevent CNC agglomeration, which reduces light dispersion and favours the transmission of visible light through the films. Notably, the PVA-ALG-10CNC exhibited the lowest light transmittance (63% at 850 nm). This behavior of the films proves the heterogeneous dispersion of CNC in the PVA-ALG-10wt% polymeric matrix, as seen by SEM analysis (Fig. 7). Additionally, several researchers have reported that the decrease in transmission level for nanocomposite films is influenced by the wt.% of the nanofiller, which can have a substantial impact on the transmittance of UV and visible light [28,29,41,56]. However, when employing bio-based nanocomposites in packaging applications, the decrease in transmission of UV-Vis radiation through the material is advantageous since UV and visible light can have a detrimental impact on the quality of food products.

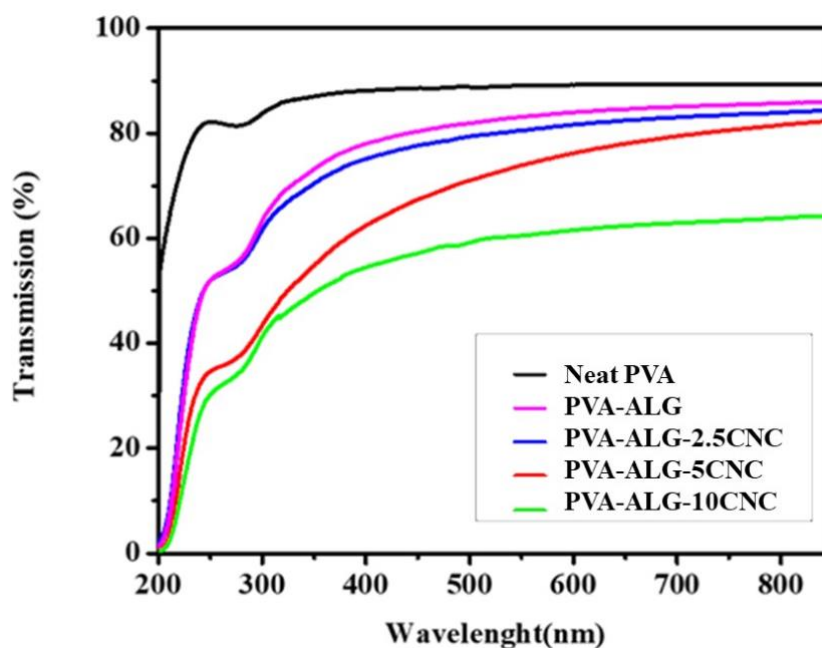


Figure 8. Photographs and UV-vis transmittance of neat PVA, PVA-ALG, and its nanocomposite films at different CNC weight fractions 2.5, 5, and 10 wt.%

3.2.5. Thermal stability of Bio-Nanocomposite Films

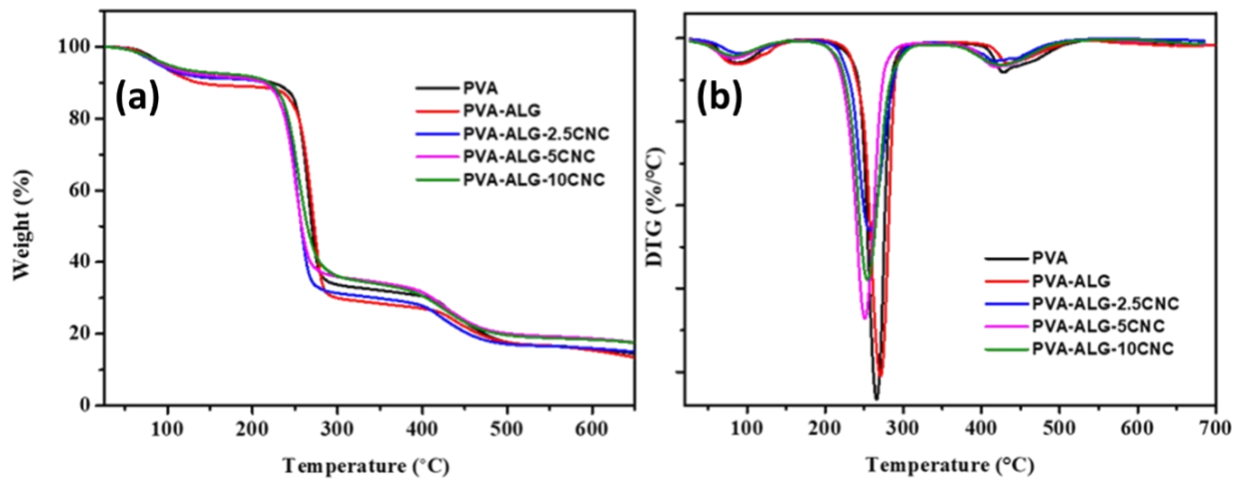


Figure 9. (a) TGA and (b) DTG curves of composite films

TGA/DTG are the most effective methods for evaluating the thermal stability of biopolymers and biopolymer-based nanocomposite films [1,25,29]. In this study, the influence of CNC on the thermal degradation of nanocomposites was evaluated using the TGA/DTG curves. Fig. 9 shows the TGA and DTG of the nanocomposite films: neat PVA, PVA-ALG blend, and PVA-ALG reinforced by 2.5, 5, and 10% of CNC. The curve of TGA shows three different steps of decomposition for all samples. The first degradation represents a 5 wt.% of loss in mass at nearly 100°C, this is due to the evaporation of physical water at the surface of the films [34,57]. The second degradation was obtained at nearly 290°C, is due to the decomposition process of the main chains of PVA, ALG, and CNC. The last step of weight loss (at about 430 °C) for all the film samples was linked to the depolymerization, deacetylation, and disintegration of units of the polymers [58]. Table 2 shows the temperature parameters for all samples (T_{onset} and T_{max}) of the major decomposition (220 to 350 °C) and the residue (R) at 600 °C that were obtained by TGA and DTG curves. It was noted that the T_{onset} and T_{max} of the nanocomposite films decreased with increasing CNC concentration. This could be due to the introduced CNC are thermally unstable nanomaterials, and as shown in Fig. 4, their disintegration process begins around 157 °C. The sulfate groups that are present on the surface of CNC are responsible for these characteristics [1,57]. The residual weight (R) values at 600 °C indicated that the residue was slightly influenced by the addition of CNC to the PVA-ALG blend. The residual weight (R) values at 600 °C indicated that the residue was slightly influenced by the addition of CNC to the PVA-ALG blend. For neat PVA and PVA-ALG blend, the residual weight was found to be 15%; for bio-nanocomposite, it was found to be between 16 and 18%. These changes in R might be caused by the good interactions between the macromolecular chains of the PVA-ALG blend and CNC as well as the sulfate groups

that are present on the surface of CNC, which might function as a catalyst for dehydration and promote the formation of char residue [11,51].

Table. 2. Temperature parameters T_{onset} ($^{\circ}\text{C}$), T_{max} ($^{\circ}\text{C}$), and R (%) at 600 $^{\circ}\text{C}$ for all samples: Neat PVA, PVA-ALG, and PVA-ALG reinforced by 2.5, 5, and 10% of CNC. obtained from TGA/DTG analysis.

Sample	T_{onset} ($^{\circ}\text{C}$)	T_{max} ($^{\circ}\text{C}$)	R at 600 $^{\circ}\text{C}$
PVA	246	266	15
PVA-ALG	250	271	15
PVA-ALG-2.5CNC	236	257	16
PVA-ALG-5CNC	233	254	19
PVA-ALG-10CNC	230	251	18

3.2.6. Mechanical Properties of Bio-Nanocomposite Films

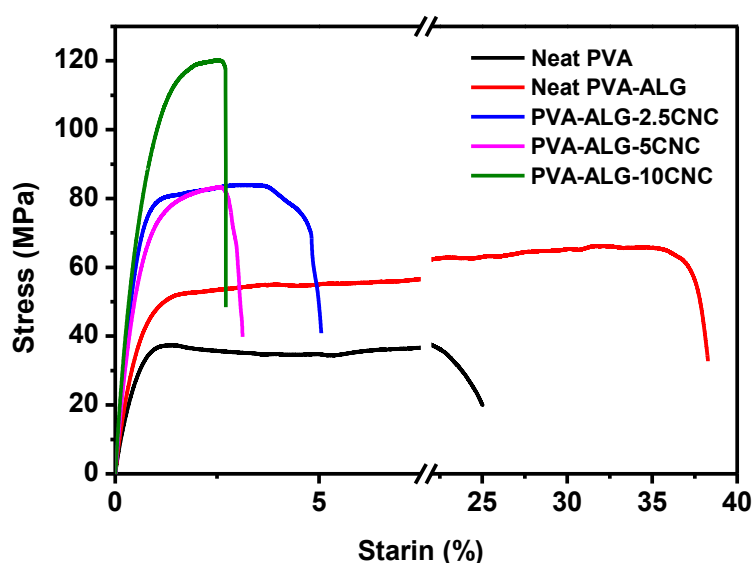


Figure 10. Tensile test of PVA-ALG based nanocomposite films at different CNC weight fraction

One of the benefit of nanotechnology filler is to improve the weak mechanical properties of pure biopolymer, herein cellulose nanocrystals were suggested as strong reinforcement because of its well established and identified properties such as high surface area and aspect ratio found to be [59]. Furthermore CNCs exhibit relatively high elastic modulus measured at 100-150 GPa [30,51,59]. In this study CNCs were added to PVA-ALG matrix with three concentration (2.5%, 5%, 10%) and their mechanical properties were evaluated and presented in Fig. 10. The young's modulus, tensile strength, and elongation at break values were summarized in Table 3. Overall, all bionanocomposites show improved mechanical properties in term of the modulus and tensile strength compared to pure biopolymers matrix, while the elongation at break decrease by the filler addition, hence as expected this latter has good effect on the mechanical properties. Neat PVA film exhibit a modulus of 44.48 MPa, a tensile strength of 40.45 MPa, and an elongation at break

of 25.08 % whereas the PVA-ALG blend present improved young's modulus (50.92 MPa), and tensile strength reaching 66.28 MPa indicating that the blend component are miscible and compatible without phase separation, while the elongation at break increased pointing out that ALG impart ductility to PVA. Moreover the bionanocomposite film filler with 10% exhibit a young's modulus of 171.77MPa and a tensile strength of 120.53 MPa which correspond 237% , and 81% increase respectively, in comparision with neat matrix these results in agreement with previous studies regarding CNC filled nanocomposites [30,41]. However, the elongation at break was decreased with 92 %. The finding in case of modulus and strength can be explained by the good interfacial interaction between the matrix blend and the reinforcement owing to the high surface area of CNCs. Besides the decrease of elongation at break comes by CNCs that restricted the chains mobility giving stiff bionanocomposites.

Table. 3. Young's Modulus, Tensile Strength, Elongation at Break of PVA-ALG based nanocomposite films at different CNC weight fraction

Samples	Young's Modulus (MPa)	Tensile Strength (MPa)	Elongation at break (%)
Neat PVA	44.48	40.45	25.08
Neat PVA-ALG	50.92	66.28	38.31
PVA-ALG-2.5CNC	115.09	83.37	5.09
PVA-ALG-5CNC	124.22	84.39	3.10
PVA-ALG-10CNC	171.77	120.53	2.75

4. Conclusion

In this work, nanocomposite films were elaborated using PVA-ALG blend as matrix and cellulose nanocrystals extracted from *Juncus* plant as a nanofiller, using casting method after a mixing process. The incorporation of CNCs into the PVA-ALG matrix blend successfully enhanced the properties of pure biopolymer which was expected. The young's modulus and tensile strength were significantly improved due to the excellent interfacial adhesion between all all-components, as shown from FTIR results. Besides, the optical transparency of the films was not affected up to 5 wt.% of CNCs, confirmed by the morphology having a homogenous dispersion at low concentration. However, the thermal stability was slightly affected by CNCs addition explained by sulfate groups that accelerated its thermal degradation.

Acknowledgment

The financial assistance of the Office Chérifien des Phosphates (OCP S.A.) in the Moroccan Kingdom toward this research is hereby acknowledged.

References

- [1] M. S. Andrade, O. H. Ishikawa, R. S. Costa, M. V. S. Seixas, R. C. L. B. Rodrigues and E. A. B. Moura, (2022). "Development of Sustainable Food Packaging Material Based on Biodegradable Polymer Reinforced with Cellulose Nanocrystals," *Food Packag. Shelf Life*, vol. 31, p. 100807. <https://doi.org/10.1016/j.fpsl.2021.100807>
- [2] H. Rajabinejad, M. Zoccola, A. Patrucco, A. Montarsolo, Y. Chen, A. Ferri, A. Muresan, and C. Tonin. (2019). "Fabrication and Properties of Keratose/Polyvinyl Alcohol Blend Films," *Polym. Bull.*, (0123456789). <https://link.springer.com/article/10.1007/s00289-019-02889-7>
- [3] S. P. Bangar, W. S. Whiteside, K. D. Dunno, G. A. Cavender, P. Dawson, and R. Love, (2022). "Starch-Based Bio-Nanocomposites Films Reinforced with Cellulosic Nanocrystals Extracted from Kudzu (*Pueraria Montana*) Vine," *Int. J. Biol. Macromol.*, vol. 203, pp. 350–360. <https://doi.org/10.1016/j.ijbiomac.2022.01.133>
- [4] K. El. Bourakadi, N. Merghoub, M. Fardioui, M. E. M. Mekhzoum, I. M. Kadmir, E. M. Essassi, A. el K. Qaiss and R. Bouhfid, (2019). "Chitosan/Polyvinyl Alcohol/Thiabendazolium-Montmorillonite Bio-Nanocomposite Films: Mechanical, Morphological and Antimicrobial Properties," *Compos. Part B Eng.*, vol. 172, pp. 103–110. <https://doi.org/10.1016/j.compositesb.2019.05.042>
- [5] M. S. Sarwar, M. B. K. Niazi, Z. Jahan, T. Ahmad and A. Hussain (2018). "Preparation and Characterization of PVA/Nanocellulose/Ag Nanocomposite Films for Antimicrobial Food Packaging," *Carbohydr. Polym.*, vol. 184, pp. 453–464. <https://doi.org/10.1016/j.carbpol.2017.12.068>
- [6] M. Gomaa, A. F. Hifney, M. A. Fawzy and K. M. Abdel-Gawad (2018), *Use of Seaweed and Filamentous Fungus Derived Polysaccharides in the Development of Alginate-Chitosan Edible Films Containing Fucoïdan: Study of Moisture Sorption, Polyphenol Release and Antioxidant Properties*, Elsevier Ltd.
- [7] A. Mittal, S. Garg and S. Bajpai (2020). "Fabrication and Characteristics of Poly (Vinyl Alcohol)-Starch-Cellulosic Material Based Biodegradable Composite Film for Packaging Application," *Materials Today: Proceedings, Elsevier Ltd*, pp. 1577–1582. <https://doi.org/10.1016/j.matpr.2019.11.210>
- [8] A. B. Perumal, P. S. Sellamuthu, R. B. Nambiar and E. R. Sadiku (2018). "Development of Polyvinyl Alcohol/Chitosan Bio-Nanocomposite Films Reinforced with Cellulose Nanocrystals Isolated from Rice Straw," *Appl. Surf. Sci.*, vol. 449, pp. 591–602. <https://doi.org/10.1016/j.apsusc.2018.01.022>
- [9] C. Zhuang, Y. Jiang, Y. Zhong, Y. Zhao, Y. Deng, J. Yue, D. Wang, S. Jiao, H. Gao, H. Chen and H. Mu (2018) "Development and Characterization of Nano-Bilayer Films Composed of Polyvinyl Alcohol, Chitosan and Alginate," *Food Control*, vol. 86, pp. 191–199. <https://doi.org/10.1016/j.foodcont.2017.11.024>
- [10] M. S. Islam, and M. R. Karim. (2010). "Fabrication and Characterization of Poly(Vinyl Alcohol)/Alginate Blend Nanofibers by Electrospinning Method," *Colloids Surfaces A Physicochem. Eng. Asp.*, vol. 366, issue. 1–3, pp. 135–140. <https://doi.org/10.1016/j.colsurfa.2010.05.038>
- [11] A. A. Oun, G. H. Shin and J. T. Kim (2022) "Antimicrobial, Antioxidant, and PH-Sensitive Polyvinyl Alcohol/Chitosan-Based Composite Films with Aronia Extract, Cellulose Nanocrystals, and Grapefruit Seed Extract," *Int. J. Biol. Macromol.*, vol. 213, pp. 381–393. <https://doi.org/10.1016/j.ijbiomac.2022.05.180>

- [12] J. Kan, J. Liu, H. Yong, Y. Liu, Y. Qin and J. Liu (2019) “Development of Active Packaging Based on Chitosan-Gelatin Blend Films Functionalized with Chinese Hawthorn (*Crataegus Pinnatifida*) Fruit Extract,” *Int. J. Biol. Macromol.*, vol. 140, pp. 384–392. <https://doi.org/10.1016/j.ijbiomac.2019.08.155>
- [13] M. El Achaby, N. El Miri, A. Aboulkas, M. Zahouily, E. Bilal, A. Barakat and A. Solhy (2017). “Processing and Properties of Eco-Friendly Bio-Nanocomposite Films Filled with Cellulose Nanocrystals from Sugarcane Bagasse,” *Int. J. Biol. Macromol.*, vol. 96, pp. 340–352. <https://doi.org/10.1016/j.ijbiomac.2016.12.040>
- [14] S. G. Kuntzler, J. A. V. Costa and M. G. de. Moraes (2018). “Development of Electrospun Nanofibers Containing Chitosan/PEO Blend and Phenolic Compounds with Antibacterial Activity,” *Int. J. Biol. Macromol.*, vol. 117, pp. 800–806. <https://doi.org/10.1016/j.ijbiomac.2018.05.224>
- [15] P. E. Fathima, S. K. Panda, P. M. Ashraf, T. O. Varghese and J. Bindu (2018). “Polylactic Acid/Chitosan Films for Packaging of Indian White Prawn (*Fenneropenaeus Indicus*),” *Int. J. Biol. Macromol.*, vol. 117, pp. 1002–1010. <https://doi.org/10.1016/j.ijbiomac.2018.05.214>
- [16] A. Arevalo-Gallegos, Z. Ahmad, M. Asgher, R. Parra-Saldivar and H. M. N. Iqbal. (2017), “Lignocellulose: A Sustainable Material to Produce Value-Added Products with a Zero Waste Approach—A Review,” *Int. J. Biol. Macromol.*, vol. 99, pp. 308–318. <https://doi.org/10.1016/j.ijbiomac.2017.02.097>
- [17] G. Guo, H. Tian and Q. Wu (2019) “Nanoclay Incorporation into Soy Protein/Polyvinyl Alcohol Blends to Enhance the Mechanical and Barrier Properties,” *Polym. Compos.*, vol. 40, issue. 9, pp. 3768–3776. <https://doi.org/10.1002/pc.25238>
- [18] M. El Achaby, Z. Kassab, A. Barakat and A. Aboulkas. (2018). “Alfa Fibers as Viable Sustainable Source for Cellulose Nanocrystals Extraction: Application for Improving the Tensile Properties of Biopolymer Nanocomposite Films,” *Ind. Crops Prod.*, vol. 112, pp. 499–510. <https://doi.org/10.1016/j.indcrop.2017.12.049>
- [19] M. Smyth, C. Rader, J. Bras and E. J. Foster. (2018) “Characterization and Mechanical Properties of Ultraviolet Stimuli-Responsive Functionalized Cellulose Nanocrystal Alginate Composites,” *J. Appl. Polym. Sci.*, vol. 135, issue. 7, pp. 1–10. <https://doi.org/10.1002/app.45857>
- [20] N. Eghbalifam, M. Frounchi and S. Dadbin. (2015). “Antibacterial Silver Nanoparticles in Polyvinyl Alcohol/Sodium Alginate Blend Produced by Gamma Irradiation,” *Int. J. Biol. Macromol.*, vol. 80, pp. 170–176. <https://doi.org/10.1016/j.ijbiomac.2015.06.042>
- [21] X. Jiang, N. Xiang, H. Zhang, Y. Sun, Z. Lin and L. Hou. (2018) “Preparation and Characterization of Poly(Vinyl Alcohol)/Sodium Alginate Hydrogel with High Toughness and Electric Conductivity,” *Carbohydr. Polym.*, vol. 186, pp. 377–383. <https://doi.org/10.1016/j.carbpol.2018.01.061>
- [22] Y. Yue, J. Han, G. Han, A. D. French, Y. Qi and Q. Wu (2016) “Cellulose Nanofibers Reinforced Sodium Alginate-Polyvinyl Alcohol Hydrogels: Core-Shell Structure Formation and Property Characterization,” *Carbohydr. Polym.*, vol. 147, pp. 155–164. <https://doi.org/10.1016/j.carbpol.2016.04.005>
- [23] N. Eghbalifam, M. Frounchi and S. Dadbin (2015) “Antibacterial Silver Nanoparticles in Polyvinyl Alcohol/Sodium Alginate Blend Produced by Gamma Irradiation,” *Int. J. Biol. Macromol.*, vol. 80, pp. 170–176. <https://doi.org/10.1016/j.ijbiomac.2015.06.042>

- [24] M. H. Salim, Y. Abdellaoui, A. Ait Benhamou, E. H. Ablouh, M. El Achaby and Z. Kassab (2022), "Influence of Cellulose Nanocrystals from Pea Pod Waste on Mechanical, Thermal, Biodegradability, and Barrier Properties of Chitosan-Based Films," *Cellulose*, vol. 29, issue. 9, pp. 5117–5135. <https://link.springer.com/article/10.1007/s10570-022-04587-6>
- [25] Y. Hua, T. Chen and Y. Tang (2022). "Preparation and Characterization of Nanocomposite Films Based on Different Ratios of Cellulose Nanocrystal and Cellulose Nanofiber," *Ind. Crops Prod.*, vol. 179, p. 114686. <https://doi.org/10.1016/j.indcrop.2022.114686>
- [26] M. El Achaby, N. El Miri, H. Hannache, S. Gmouh, V. Trabadelo, A. Aboulkas and H. Ben Youcef. (2018) "Cellulose Nanocrystals from Miscanthus Fibers: Insights into Rheological, Physico-Chemical Properties and Polymer Reinforcing Ability," *Cellulose*, vol. 25, issue. 11, pp. 6603–6619. <https://link.springer.com/article/10.1007/s10570-018-2047-1>
- [27] F. Luzi, D. Puglia, F. Sarasini, J. Tirillò, G. Maffei, A. Zuorro, R. Lavecchia, J. M. Kenny and L. Torre (2019) "Valorization and Extraction of Cellulose Nanocrystals from North African Grass: *Ampelodesmos Mauritanicus* (Diss)," *Carbohydr. Polym.*, vol. 209, pp. 328–337. <https://doi.org/10.1016/j.carbpol.2019.01.048>
- [28] M. Yadav and F. C. Chiu. (2019). "Cellulose Nanocrystals Reinforced κ -Carrageenan Based UV Resistant Transparent Bionanocomposite Films for Sustainable Packaging Applications," *Carbohydr. Polym.*, vol. 211, pp. 181–194. <https://doi.org/10.1016/j.carbpol.2019.01.114>
- [29] M. H. Salim, Z. Kassab, Y. Abdellaoui, A. García - Cruz, A. Soumare, E. Ablouh, houssaine and M. El Achaby (2022) "Exploration of Multifunctional Properties of Garlic Skin Derived Cellulose Nanocrystals and Extracts Incorporated Chitosan Biocomposite Films for Active Packaging Application," *Int. J. Biol. Macromol.*, vol. 210, pp. 639–653. <https://doi.org/10.1016/j.ijbiomac.2022.04.220>
- [30] H. A. Silvério, W. P. Flauzino Neto, N. O. Dantas and D. Pasquini. (2013) "Extraction and Characterization of Cellulose Nanocrystals from Corn cob for Application as Reinforcing Agent in Nanocomposites," *Ind. Crops Prod.*, vol. 44, pp. 427–436. <https://doi.org/10.1016/j.indcrop.2012.10.014>
- [31] M. C. Popescu. (2017) "Structure and Sorption Properties of CNC Reinforced PVA Films," *Int. J. Biol. Macromol.*, vol. 101, pp. 783–790. <https://doi.org/10.1016/j.ijbiomac.2017.03.168>
- [32] K. S. Prado and M. A. S. Spinacé. (2019), "Isolation and Characterization of Cellulose Nanocrystals from Pineapple Crown Waste and Their Potential Uses," *Int. J. Biol. Macromol.*, vol. 122, pp. 410–416. <https://doi.org/10.1016/j.ijbiomac.2018.10.187>
- [33] W. Lei, C. Fang, X. Zhou, Q. Yin, S. Pan, R. Yang, D. Liu and Y. Ouyang. (2018). "Cellulose Nanocrystals Obtained from Office Waste Paper and Their Potential Application in PET Packing Materials," *Carbohydr. Polym.*, vol. 181, pp. 376–385. <https://doi.org/10.1016/j.carbpol.2017.10.059>
- [34] J. Prasad Reddy and J. W. Rhim. (2014). "Isolation and Characterization of Cellulose Nanocrystals from Garlic Skin," *Mater. Lett.*, vol. 129, pp. 20–23. <https://doi.org/10.1016/j.matlet.2014.05.019>
- [35] D. Chen, D. Lawton, M. R. Thompson and Q. Liu. (2012). "Biocomposites Reinforced with Cellulose Nanocrystals Derived from Potato Peel Waste," *Carbohydr. Polym.*, vol. 90, issue. 1, pp. 709–716. <https://doi.org/10.1016/j.carbpol.2012.06.002>
- [36] N. El Miri, K. Abdelouahdi, M. Zahouily, A. Fihri, A. Barakat, A. Solhy and M. El Achaby.

- (2015). "Bio-Nanocomposite Films Based on Cellulose Nanocrystals Filled Polyvinyl Alcohol/Chitosan Polymer Blend," *J. Appl. Polym. Sci.*, vol. 132, issue. 22, pp. 1–13. <https://doi.org/10.1002/app.42004>
- [37] G. E. Luckachan and C. K. S. Pillai. (2011). "Biodegradable Polymers- A Review on Recent Trends and Emerging Perspectives," *J. Polym. Environ.*, vol. 19, issue. 3, pp. 637–676. <https://link.springer.com/article/10.1007/s10924-011-0317-1>
- [38] A. Nugroho, Basyirun, R. Mamat, J. P. Siregar, D. Widjanarko and Ramelan. (2020) "Microstructure and Physical of Al₂O₃ 2SiO₄ 2H₂O Kaolinite Particle Analysis by Shacking Time and Powder Metallurgy," *Scitepress*, pp. 48–53.
- [39] Z. Kassab, M. El Achaby, Y. Tamraoui, H. Sehaqui, R. Bouhfid and A. E. K. Qaiss (2019). "Sunflower Oil Cake-Derived Cellulose Nanocrystals: Extraction, Physico-Chemical Characteristics and Potential Application," *Int. J. Biol. Macromol.*, vol. 136, pp. 241–252. <https://doi.org/10.1016/j.ijbiomac.2019.06.049>
- [40] L. Van Hai, H. N. Son and Y. B. Seo. (2015) "Physical and Bio-Composite Properties of Nanocrystalline Cellulose from Wood, Cotton Linters, Cattail, and Red Algae," *Cellulose*, vol. 22, issue. 3, pp. 1789–1798. <https://link.springer.com/article/10.1007/s10570-015-0633-z>
- [41] S. Thambiraj and D. Ravi Shankaran. (2017). "Preparation and Physicochemical Characterization of Cellulose Nanocrystals from Industrial Waste Cotton," *Appl. Surf. Sci.*, vol. 412, pp. 405–416. <https://doi.org/10.1016/j.apsusc.2017.03.272>
- [42] F. Luzi, E. Fortunati, D. Puglia, M. Lavorgna, C. Santulli, J. M. Kenny and L. Torre. (2014). "Optimized Extraction of Cellulose Nanocrystals from Pristine and Carded Hemp Fibres," *Ind. Crops Prod.*, vol. 56, pp. 175–186. <https://doi.org/10.1016/j.indcrop.2014.03.006>
- [43] M. Mujtaba, A. M. Salaberria, M. A. Andres, M. Kaya, A. Gunyakti and J. Labidi. (2017). "Utilization of Flax (*Linum Usitatissimum*) Cellulose Nanocrystals as Reinforcing Material for Chitosan Films," *Int. J. Biol. Macromol.*, vol. 104, pp. 944–952. <https://doi.org/10.1016/j.ijbiomac.2017.06.127>
- [44] Q. Lu, lin, L. Tang, rong, S. Wang, B. Huang, Y. Chen and X. Chen, rong. (2014) "An Investigation on the Characteristics of Cellulose Nanocrystals from *Pennisetum Sinese*," *Biomass and Bioenergy*, vol. 70, pp. 267–272. <https://doi.org/10.1016/j.biombioe.2014.09.012>
- [45] Z. Kassab, I. Kassem, H. Hannache, R. Bouhfid, A. E. K. Qaiss and M. El Achaby (2020). "Tomato Plant Residue as New Renewable Source for Cellulose Production: Extraction of Cellulose Nanocrystals with Different Surface Functionalities," *Cellulose*, vol. 7, pp. 1–17. <https://link.springer.com/article/10.1007/s10570-020-03097-7>
- [46] A. A. Oun and J. W. Rhim. (2016), "Characterization of Nanocelluloses Isolated from Ushar (*Calotropis Procera*) Seed Fiber: Effect of Isolation Method," *Mater. Lett.*, vol. 168, pp. 146–150. <https://doi.org/10.1016/j.matlet.2016.01.052>
- [47] A. Y. Melikoğlu, S. E. Bilek and S. Cesur. (2019) "Optimum Alkaline Treatment Parameters for the Extraction of Cellulose and Production of Cellulose Nanocrystals from Apple Pomace," *Carbohydr. Polym.*, vol. 215, pp. 330–337. <https://doi.org/10.1016/j.carbpol.2019.03.103>
- [48] N. El Miri, F. Aziz, A. Aboulkas, M. El Bouchti, H. Ben Youcef and M. El Achaby. (2018). "Effect of Plasticizers on Physicochemical Properties of Cellulose Nanocrystals Filled Alginate Bionanocomposite Films," *Adv. Polym. Technol.*, vol. 37, issue. 8, pp. 3171–3185.

<https://doi.org/10.1002/adv.22087>

- [49] Z. Kassab, A. Boujemaoui, H. Ben Youcef, A. Hajlane, H. Hannache and M. El Achaby. (2019), "Production of Cellulose Nanofibrils from Alfa Fibers and Its Nanoreinforcement Potential in Polymer Nanocomposites," *Cellulose*, vol. 26, issue. 18, pp. 9567–9581. <https://link.springer.com/article/10.1007/s10570-019-02767-5>
- [50] K. Sahlin, L. Forsgren, T. Moberg, D. Bernin, M. Rigdahl and G. Westman. (2018). "Surface Treatment of Cellulose Nanocrystals (CNC): Effects on Dispersion Rheology," *Cellulose*, vol. 25, issue. 1, pp. 331–345. <https://link.springer.com/article/10.1007/s10570-017-1582-5>
- [51] A. B. Perumal, R. B. Nambiar, P. S. Sellamuthu, E. R. Sadiku, X. Li and Y. He. (2022) "Extraction of Cellulose Nanocrystals from Areca Waste and Its Application in Eco-Friendly Biocomposite Film," *Chemosphere*, vol. 287, p. 132084. <https://doi.org/10.1016/j.chemosphere.2021.132084>
- [52] M. Yang, L. Li, S. Yu, J. Liu and J. Shi. (2020). "High Performance of Alginate/ Polyvinyl Alcohol Composite Film Based on Natural Original Melanin Nanoparticles Used as Food Thermal Insulating and UV–Vis Block," *Carbohydr. Polym.*, vol. 233, p. 115884. <https://doi.org/10.1016/j.carbpol.2020.115884>
- [53] B. Sharma, P. Malik and P. Jain. (2018). "Biopolymer Reinforced Nanocomposites: A Comprehensive Review," *Mater. Today Commun.*, vol. 16, pp. 353–363. <https://doi.org/10.1016/j.mtcomm.2018.07.004>
- [54] A. Nugroho, Z. Bo, R. Mamat, W. H. Azmi, G. Najafi and F. Khoirunnisa. (2021). "Extensive Examination of Sonication Duration Impact on Stability of Al₂O₃-Polyol Ester Nanolubricant," *Int. Commun. Heat Mass Transf.*, vol. 126, p. 105418. <https://doi.org/10.1016/j.icheatmasstransfer.2021.105418>
- [55] A. Nugroho, R. Mamat, Z. Bo, W. H. Azmi, R. Alenezi and G. Najafi. (2022). "An Overview of Vapor Compression Refrigeration System Performance Enhancement Mechanism by Utilizing Nanolubricants," *J. Therm. Anal. Calorim.*, vol. 147, issue. 17, pp. 9139–9161. <https://link.springer.com/article/10.1007/s10973-022-11230-w>
- [56] P. Cazón, G. Velázquez and M. Vázquez. (2020). "Regenerated Cellulose Films Combined with Glycerol and Polyvinyl Alcohol: Effect of Moisture Content on the Physical Properties," *Food Hydrocoll.*, vol. 103, p. 105657. <https://doi.org/10.1016/j.foodhyd.2020.105657>
- [57] J. Prasad Reddy and J. W. Rhim (2014). "Isolation and Characterization of Cellulose Nanocrystals from Garlic Skin," *Mater. Lett.*, vol. 129, pp. 20–23.
- [58] L. Chen, Q. Wang, K. Hirth, C. Baez, U. P. Agarwal and J. Y. Zhu. (2015). "Tailoring the Yield and Characteristics of Wood Cellulose Nanocrystals (CNC) Using Concentrated Acid Hydrolysis," *Cellulose*, vol. 22, issue. 3, pp. 1753–1762. <https://link.springer.com/article/10.1007/s10570-015-0615-1>
- [59] P. Dhar, D. Tarafder, A. Kumar and V. Katiyar. (2015). "Effect of Cellulose Nanocrystal Polymorphs on Mechanical, Barrier and Thermal Properties of Poly(Lactic Acid) Based Bionanocomposites," *RSC Adv.*, vol. 5, issue. 74, pp. 60426–60440. <https://pubs.rsc.org/en/content/articlelanding/2015/ra/c5ra06840a/unauth>